Multiscale Modeling of Shear-Dependent Tumor Cell Adhesion

Aristotle Martin[1 [0000−0002−8704−764X]], Mohammed Shihab Kabir[1 [0009−0008−1743−4581]], Runxin Wu[1 [0009−0008−1945−413X]], and Amanda Randles[1 [0000−0001−6318−3885]]

Dept of Biomedical Engineering, Duke University, Durham NC 27705, USA
{aristotle.martin, shihab.kabir, wendy.wu, amanda.randles}@duke.edu

Abstract. Circulating tumor cells (CTCs) interact with the vascular endothelium under hemodynamic forces that influence where metastatic seeding occurs. Wall shear stress (WSS) has been shown to regulate adhesive signaling, yet its mechanistic role in shaping spatial patterns of CTC arrest within complex vascular networks remains poorly understood. In this work, we present a three dimensional multiscale simulation framework that couples tissue scale blood flow with receptor ligand adhesive dynamics whose kinetics depend on local WSS. We evaluate three modes of WSS regulation, including modulation by WSS magnitude, modulation by the local spatial gradient of WSS, and modulation by peak upstream WSS gradient within a region of influence. Using physiologically realistic vessel geometries and flow conditions, we track thousands of CTCs across tissue scale vascular networks using a high throughput adaptive refinement strategy executed on the Aurora supercomputer. Across a curved microvessel and a reconstructed bioprinted double bifurcation network, WSS magnitude dependent adhesion produces strong spatial biases in CTC arrest. In the bioprinted network, inclusion of WSS regulated adhesion leads to a thirty one fold increase in active receptor engagement in the lower entry fork compared to a non WSS modulated baseline, consistent with experimentally observed regional enrichment. These results demonstrate that local WSS profiles act as a physical driver of preferential CTC attachment and motivate inclusion of shear regulated adhesion in predictive models of metastatic transport.

Keywords: Metastasis · Wall shear stress · Multiscale modeling · Adhesive dynamics.

1 Introduction

Predicting where circulating tumor cells (CTCs) arrest and adhere within the vascular system requires a mechanistic understanding of how hemodynamic forces and adhesive signaling interact during transport. Metastasis remains the primary cause of cancer related mortality worldwide [1], with strong correlations between the cancer subtype and the preferred metastatic site, such as prostate

ICCS Camera Ready Version 2026
To cite this paper please use the final published version:
DOI: 10.1007/978-3-032-29921-5_30

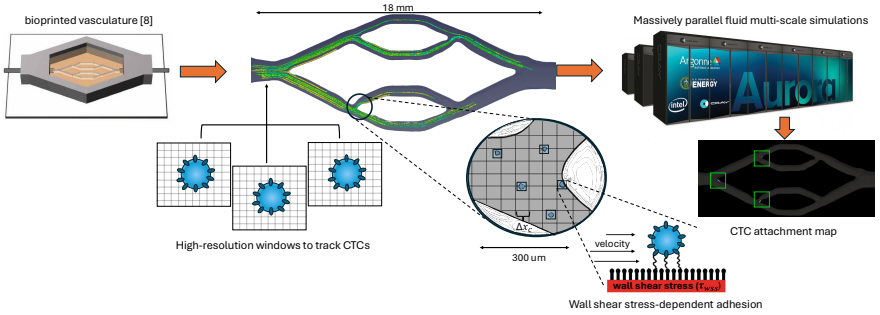

Fig. 1. Overview of the experimental pipeline for *in silico* tracking of circulating tumor cells in a tissue-scale vascular network. The bioprinted vasculature from Hynes et al. [17] is converted to a computational mesh that is supplied to the multi-scale physics solver, HARVEY [32]. High-resolution windows are used to track the trajectories of thousands of adhesive circulating tumor cells in parallel. Each tumor cell undergoes wall shear stress-modulated adhesive interactions with receptor-lined endothelium. These large-scale simulations are conducted on the Aurora supercomputer (Argonne National Laboratory). HARVEY generates the cell attachment maps that inform metastatic preferences of circulating tumor cells.

cancer to bone, pancreatic cancer to liver, and breast cancer to brain or lungs [13, 6, 12, 15]. Two complementary hypotheses have historically framed organ specific metastasis. James Ewing's anatomical hypothesis emphasizes the role of vascular geometry and blood flow in the direction of CTC trajectories [10], while Stephen Paget's seed and soil hypothesis argues that colonization depends on biochemical compatibility between tumor cells and target tissue [26]. Although advances in cell adhesion biology have provided strong support for the seed and soil paradigm, the expression of adhesion molecules alone does not fully explain the observed metastatic patterns.

Recent experimental studies suggest that local hemodynamics play a critical role in shaping where CTCs attach. Perfusion experiments by Hynes et al. revealed pronounced regional preferences in the attachment of metastatic mammary carcinoma cells to bioprinted microvascular networks, despite uniform expression of adhesion molecules [17]. In particular, these attachment hotspots coincided with regions of distinct wall shear stress (WSS), the tangential force exerted by blood flow on the vascular endothelium. Previous work has shown that WSS can promote or inhibit CTC adhesion depending on magnitude and spatial variation [37, 9, 5], particularly near bends and bifurcations. However, isolating the mechanistic contribution of WSS to population scale CTC arrest remains challenging, as resolving three dimensional flow, cell mechanics, and adhesive interactions over physiologically relevant vascular distances is computationally prohibitive in experimental and numerical settings [7, 18].

In this work, we address this gap by introducing the first population scale, three dimensional multiscale computational framework that couples tissue scale

ICCS Camera Ready Version 2026
To cite this paper please use the final published version:
DOI: 10.1007/978-3-032-29921-5_30

blood flow with WSS dependent receptor ligand adhesive kinetics. By integrating shear regulated adhesive dynamics into a high throughput adaptive refinement strategy, we track thousands of individual CTCs across realistic vascular geometries while resolving submicrometer binding interactions. This approach enables direct, quantitative testing of how different modes of WSS regulation influence spatial patterns of CTC arrest, providing a mechanistic link between local hemodynamics and preferential metastatic attachment.

2 Materials and Methods

2.1 Computational Fluid Dynamics via the Lattice Boltzmann Method

We simulate incompressible blood flow using the lattice Boltzmann method (LBM), implemented in HARVEY [32]. The fluid is advanced with the single relaxation time Bhatnagar Gross Krook collision operator on a standard D3Q19 lattice [31, 4]. The update for distribution f_i at position $\mathbf{x}$ and time t with discrete velocity $\mathbf{c}_i$, relaxation time τ, and forcing term F_i is

$$f_i(\mathbf{x}+\mathbf{c}_i, t+1) = \left(1-\frac{1}{\tau}\right) f_i(\mathbf{x},t) + \frac{1}{\tau} f_i^{eq}(\mathbf{x},t) + F_i(\mathbf{x},t). \tag{1}$$

2.2 Cell Mechanics via a Membrane Finite Element Model

Circulating tumor cells are modeled as deformable, fluid filled capsules with triangulated membranes generated by successive subdivision of an icosahedron. Membrane mechanics are resolved with a finite element formulation [19] and the Skalak constitutive law [34], which captures resistance to shear, bending, and area dilation.

2.3 Fluid Structure Interaction via the Immersed Boundary Method

Fluid structure interaction is handled with an immersed boundary method (IBM) [27] that couples the Lagrangian cell membrane to the Eulerian fluid grid [19]. Let $\delta(\cdot)$ denote a compact support interpolation kernel. During interpolation, the fluid velocity $\mathbf{V}$ at a membrane point $\mathbf{X}$ is obtained from neighboring fluid velocities $\mathbf{v}$ as

$$\mathbf{V}(\mathbf{X},t) = \sum_{\mathbf{x}} \mathbf{v}(\mathbf{x},t)\, \delta(\mathbf{x}-\mathbf{X}(t))\,. \tag{2}$$

Membrane forces $\mathbf{G}$ computed by the finite element model are then spread back to the fluid as

$$\mathbf{g}(\mathbf{x},t) = \sum_{\mathbf{X}} \mathbf{G}(\mathbf{X},t)\, \delta(\mathbf{x}-\mathbf{X}(t))\,. \tag{3}$$

ICCS Camera Ready Version 2026
To cite this paper please use the final published version:
DOI: 10.1007/978-3-032-29921-5_30

2.4 Ligand Receptor Adhesion via Adhesive Dynamics

Cell wall adhesion is modeled with stochastic adhesive dynamics [16]. Bond formation (k_f) and rupture (k_r) follow force dependent kinetics [11]:

$$k_f = k_{f_0} \exp\left(-\frac{\sigma_{on}(\ell - \lambda)^2}{2k_B T}\right), \tag{4}$$

$$k_r = k_{r_0} \exp\left(\frac{\sigma_{off}(\ell - \lambda)^2}{2k_B T}\right), \tag{5}$$

where ℓ is the bond length, λ is the equilibrium length, σ_{on} and σ_{off} are bond strengths, and $k_B T$ has its usual meaning. Once formed, each bond is modeled as a Hookean spring with stiffness k_b:

$$\boldsymbol{F}_b = -k_b(\ell - \lambda)\,\frac{\boldsymbol{\ell}_{ij}}{\ell}. \tag{6}$$

Equations 4–5 define the baseline adhesion model (Model 0) used when adhesion kinetics are not regulated by wall shear stress.

2.5 Wall Shear Stress Regulated Adhesive Kinetics

We evaluate three modes of wall shear stress (WSS) regulation of adhesion, adapted from Yan et al. [38]. Model 1 modulates kinetics using the WSS magnitude. Model 2 modulates kinetics using the directional derivative of WSS along the local flow direction at the wall. Model 3 uses the peak upstream directional derivative within a region of influence (ROI), producing a step like response downstream of the first strong gradient encountered.

Model 1: WSS magnitude regulation. With WSS magnitude σ_w and reference value σ_{w0},

$$k_f = k_f^n \left(\frac{\sigma_w}{\sigma_{w0}}\right)^{k_1}, \tag{7}$$

$$k_r = k_r^n \left(\frac{\sigma_w}{\sigma_{w0}}\right)^{k_2}. \tag{8}$$

Models 2 and 3: three dimensional WSS gradient regulation. To generalize the one dimensional formulation to three dimensions, we replace the axial derivative with a directional derivative computed from the WSS gradient $\nabla\sigma_w$ and the unit tangent $\mathbf{t}$ aligned with the local flow direction along the wall:

$$k_f = k_f^n \exp(k_3\,(\nabla\sigma_w \cdot \mathbf{t}))\,, \tag{9}$$

$$k_r = k_r^n \exp(k_4\,(\nabla\sigma_w \cdot \mathbf{t}))\,. \tag{10}$$

For Model 3, the modulation uses the maximum or minimum directional derivative within a region of influence around the upstream peak location:

$$k_f = k_f^n \exp\Big(k_3 \max_{\text{ROI}}(\nabla\sigma_w \cdot \mathbf{t})\Big)\,, \tag{11}$$

ICCS Camera Ready Version 2026
To cite this paper please use the final published version:
DOI: 10.1007/978-3-032-29921-5_30

$$k_r = k_r^n \exp\Big(k_4 \min_{\text{ROI}}(\nabla\sigma_w \cdot \mathbf{t})\Big). \tag{12}$$

We estimate $\nabla\sigma_w$ at wall adjacent fluid nodes using a local least squares fit after sliding window smoothing [2].

2.6 Multi-Resolution Coupling with Adaptive Physics Refinement

The adaptive physics refinement (APR) framework enables resolving fine-grained cellular interactions over large spatial distances using a high-resolution "moving window" to track cancer cells coupled to a bulk fluid flow in a coarsely resolved domain outside the window [30]. The moving window is a rectangular prism placed by the user at a specified location of the vascular geometry at the start of the simulation, centered around a CTC to be tracked. Within the window, high-resolution grids are used to resolve fluid-structure interactions of the deformable cell, while a coarser grid is employed outside the window to resolve the background fluid dynamics. The APR method is optimized for heterogeneous workloads, with the bulk computations performed by the CPUs, and the fine window calculations done by the GPUs. A detailed discussion of the methods underpinning APR can be found in [30, 24]. We recently extended APR to accommodate multiple simultaneous windows for high-throughput tracking of cancer cells [23].

2.7 Parameter Selection and in Silico Experiment Design

Adhesion parameters were selected based on literature values. A bond spring constant of $k_b = 10^{-3}\,\mathrm{N/m}$ was adopted based on experimental estimates of selectin bond stiffness in leukocyte adhesive dynamics studies [16, 22, 33], which characterize molecular interactions analogous to those implicated in CTC–endothelium attachment. For adhesive kinetics, the selected reverse rate $k_r = 25\,\mathrm{s}^{-1}$ is consistent with the order of magnitude of slip-bond dissociation rates reported for P-selectin under force [22], and was chosen to reflect the accelerated turnover expected under elevated shear stresses relevant to CTC attachment. The parameters controlling WSS-mediated regulation of adhesive kinetics were informed by the formulation of Yan et al. [38] and modified to support three-dimensional vessel geometries. The normalization factor σ_{w0} was selected to reflect the characteristic WSS magnitudes observed in the curved microvessel (Fig. 2). For the curved microvessel experiments, an inlet velocity of 1.5 mm/s was used, consistent with physiological flow speeds commonly reported in post-capillary venules [28]. A summary of these simulation parameters can be found in Table 1.

For all simulations, fluid flow was first advanced to steady state prior to introducing CTCs. In the double-bifurcation experiments based on Hynes et al. [17], we initialized 3,072 CTCs randomly near the vessel inlet, with one APR window assigned to track each cell. This sample size was selected to ensure robust statistical characterization of rare adhesion events while maintaining full utilization of available hardware—specifically, one GPU per CTC across 512 Aurora nodes equipped with six GPUs each ($6 \times 512 = 3{,}072$). Each APR

ICCS Camera Ready Version 2026
To cite this paper please use the final published version:
DOI: 10.1007/978-3-032-29921-5_30

window is one-way coupled to the bulk fluid, an assumption that was validated in [23]. Thus, after allowing the bulk to reach convergence, each CTC is tracked independently of other cells. To track CTC residence time, two metrics are used: occupancy and binding time. The occupancy measure was introduced in [25] and tracks the number of time steps for which a fluid point is deemed inside the CTC. To aggregate CTC occupancies while accounting for crossing paths, a mean residence time τ_{res} is computed by scaling the cumulative occupancy by the number of unique CTCs crossing a given point $N_{CTC_{x,y,z}}$ at each grid location (Equation 13).

$$\tau_{res} = \frac{\sum_{i=1}^{N_{windows}} Occupancy_{x,y,z}}{N_{CTC_{x,y,z}}} \tag{13}$$

The binding time is computed by tracking the number of time steps that each endothelial receptor is actively engaged with a CTC ligand.

Parameter Name	Symbol	Value	Reference
Bond spring constant	k_b	1×10^{-3} N/m	Section 2.7
Forward bond strength	σ_{on}	0.5×10^{-6} N/m	[29]
Reverse bond strength	σ_{off}	5×10^{-6} N/m	[29]
Forward rate constant	k_{f_o}	1×10^{4} s^{-1}	[36]
Reverse rate constant	k_{r_0}	25 s^{-1}	Section 2.7
Equilibrium bond length	λ	0.5×10^{-6} m	[35]
Cutoff length for formation	H_c	1.0×10^{-6} m	[35]
WSS bond formation sensitivity	k_1	5.5	Section 2.7
WSS bond rupture sensitivity	k_2	-10.0	Section 2.7
∇WSS bond formation sensitivity	k_3	1.0×10^{-5} m^3/N	Section 2.7
∇WSS bond rupture sensitivity	k_4	-2.5×10^{-6} m^3/N	Section 2.7
Reference shear stress	σ_{w0}	1.0	Section 2.7
Fluid velocity	v	1.5 mm/s, 1690 µL/min†	Section 2.7
Shear modulus	G_s	1×10^{-5} N/m	[17]
Ligand density	N_l	5×10^{12}/m^2	[29]
Receptor density	N_r	4.6×10^{12}/m^2	[36]

Table 1. Adhesive Dynamics and Flow Parameters Used in Simulations. †Value based on experimental conditions reported in [17].

3 Results

3.1 Adhesive Cell Behavior is Strongly Dependent on Wall Shear Stress Modulation

To investigate how different modes of WSS modulation influence adhesive transport, the three models outlined in Section 2.5 were evaluated within a curved microvessel geometry. For clarity, we denote the baseline, non-WSS-modulated

ICCS Camera Ready Version 2026
To cite this paper please use the final published version:
DOI: 10.1007/978-3-032-29921-5_30

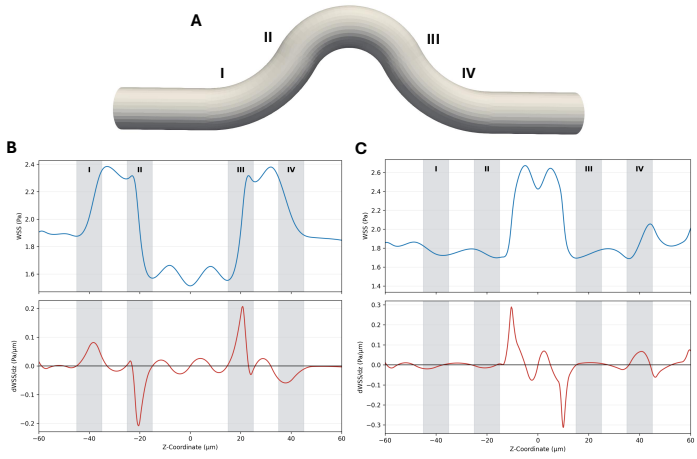

Fig. 2. (A): 3D representation of the curved microvessel, with inflection points denoted by roman numerals. (B): Cross-sectional wall shear stress (blue) and ∇(WSS) (red) plotted along the upper vessel wall. (C): Cross-sectional wall shear stress (blue) and ∇(WSS) (red) plotted along the lower vessel wall.

case as Model 0 and the WSS-modulated schemes in Fig. 3(A–C) as Models 1–3 in all subsequent discussion.

Curvature-induced secondary flows generate localized regions of elevated WSS and strong positive or negative WSS gradients, providing a biomechanical context relevant to CTC adhesion [14]. The geometry used, along with corresponding WSS and WSS-gradient traces along the upper wall of the microvessel, are shown in Fig. 2. Regions of vascular bending are denoted by Roman numerals to highlight locations where abrupt changes in WSS occur and where preferential CTC adhesion might arise.

The modulation of receptors by WSS is visualized for each mode of WSS in Fig. 3. With receptor modulation being driven by the scalar magnitude of WSS (Model 1) as shown in Fig. 3(A), the regional bond formation hotspots coincide with elevated WSS, consistent with the WSS plot in Fig. 2. Under the WSS-gradient-sensitive model (Model 2), bond formation hotspots coincide with rapidly increasing WSS (Fig. 3(B)). Conversely, the rate of bond formation is inhibited at the regions of rapid decrease in WSS. Modulation of the binding on-rate using Model 3 yields a step-like function where the modulation factor retains a peak value downstream of the first spike encountered at the lower wall (Fig. 3(C)).

Simulations of CTC transport through the curved microvessel were performed for a non-WSS-mediated baseline and compared against the three WSS-mediated adhesion models. The effects of WSS modulation on adhesive transport are quantified via binding frequency (Fig. 6), cell speed (Fig. 5), and binding duration

ICCS Camera Ready Version 2026
To cite this paper please use the final published version:
DOI: 10.1007/978-3-032-29921-5_30

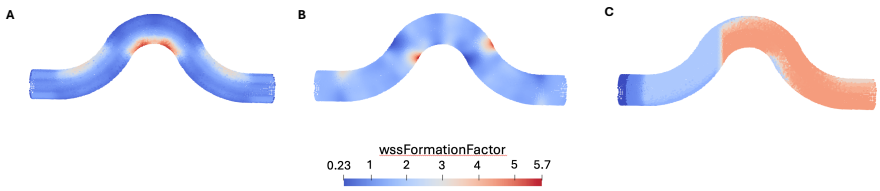

Fig. 3. Visualization of the WSS modulation factor at wall receptors locations in the curved microvessel geometry. (A): Modulation by the scalar magnitude of WSS (Model 1). (B): Modulation by the instantaneous magnitude of the spatial gradient of WSS (Model 2). (C): Modulation by the peak upstream value of the spatial gradient of WSS (Model 3).

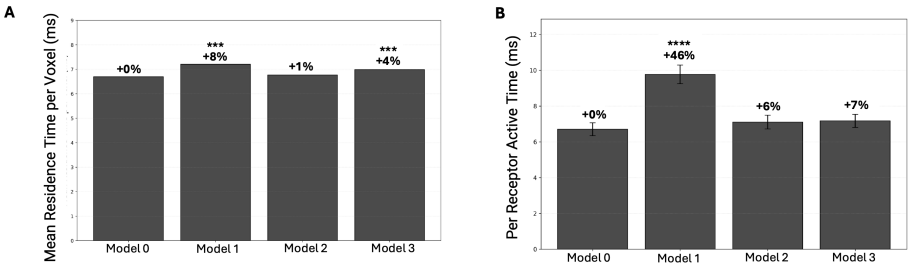

Fig. 4. Comparison of (A): mean residence time per voxel, and (B): mean bond active time per receptor.

(Fig. 4). In Fig. 6(A), the total number of adhesive bonds formed along the axial direction is quantified for each model. The cumulative number of binding events is plotted for each model in Fig. 6(B). Statistical analysis (ANOVA with Tukey HSD post-hoc testing) shows that WSS-regulated adhesion significantly increases the total number of bond-formation events relative to the non-WSS baseline (Model 1: +28%, Model 3: +18%; $p < 0.05$), whereas Model 2 remains significantly different from baseline. From Fig. 5, mean CTC velocity showed a modest yet statistically significant (5%) reduction exclusively under Model 1, while Models 2–3 remained statistically indistinguishable from baseline. Adhesive residence time (Fig. 4) is evaluated using two complementary measures. Figure 4(A) shows the mean residence time per voxel, representing the cumulative time the CTC overlaps with each fluid point. Meanwhile, Fig. 4(B) quantifies the mean duration for which each endothelial receptor remains bound to the CTC. Statistical evaluation of adhesion kinetics revealed that WSS-dependent adhesion (Models 1 and 3) significantly increased both the frequency and duration of adhesive events ($p < 0.001$), with Model 1 producing the largest enhancement in per-receptor binding lifetime (+46%) and per-voxel residence time (+8%).

ICCS Camera Ready Version 2026
To cite this paper please use the final published version:
DOI: 10.1007/978-3-032-29921-5_30

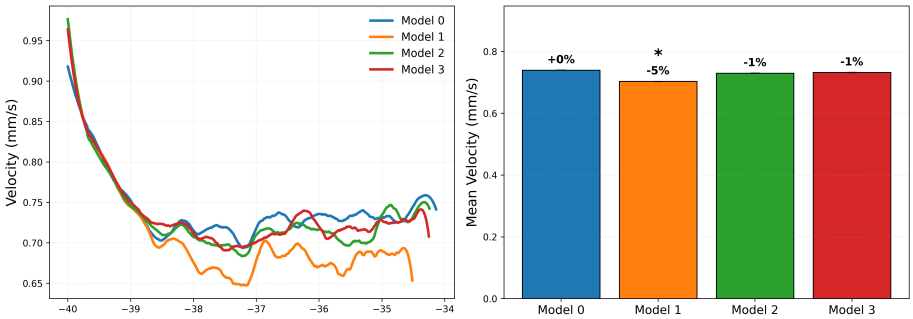

Fig. 5. Comparison of (A) cell velocity in the curved microvessel, and (B) average velocity among all WSS models.

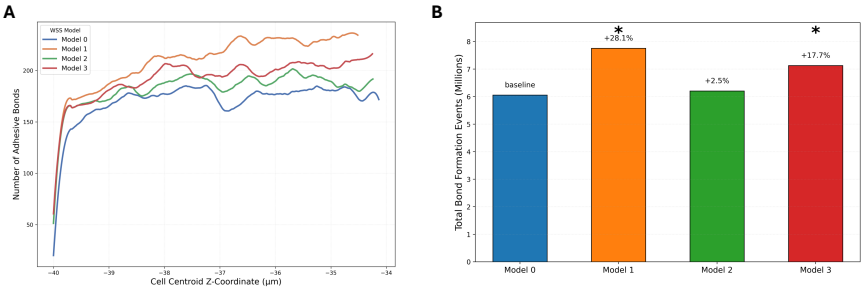

Fig. 6. Comparison of (A) number of adhesive bonds formed with axial position, and (B) total number of binding events, in millions, among each WSS model.

3.2 Wall Shear Stress-Dependent Adhesion Underlies Regional Preferences for Cell Attachment

Regional preferences for CTC attachment have been observed experimentally, yet the mechanistic role of WSS remains difficult to resolve.

Hynes et al. [17] reported preferential bond formation at the lower entry fork of a double-bifurcating vessel in a bioprinted microvessel model and posited that asymmetric WSS patterns may contribute to this behavior. However, direct testing of this mechanism remained out of reach: explicitly resolving 3-D, submicrometer adhesive interactions over physiologically relevant vessel lengths imposes prohibitive computational demands—requiring hundreds of terabytes of storage and tens of thousands of processors [23]. These constraints motivated the development of our multiscale CTC-tracking platform (Fig. 1). By incorporating WSS-dependent adhesion into this framework, we can now investigate the mechanistic links between WSS and spatial patterns of metastatic cell attachment that were previously inaccessible. To assess whether WSS drives the preferential

ICCS Camera Ready Version 2026
To cite this paper please use the final published version:
DOI: 10.1007/978-3-032-29921-5_30

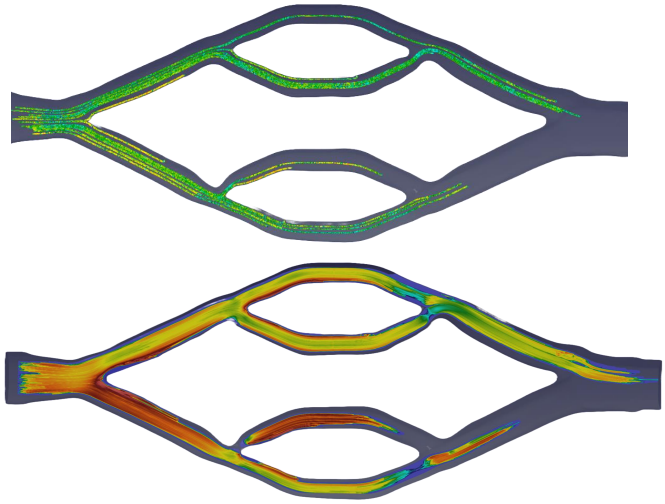

Fig. 7. (A): Subset of CTC trajectories in the double-bifurcation geometry, colored by local residence time. Brighter regions (yellow) indicate locations where cells spent longer durations in close proximity to the vessel wall. (B): Mean residence time aggregated across all simulated CTCs, with darker brown corresponding to higher average dwell times across cells. Some trajectories terminate before reaching the outlet, as only regions proximal to the inlet bifurcations exhibited WSS-dependent adhesion behavior, and downstream segments were therefore not simulated to completion.

binding patterns reported by Hynes et al. [17], we simulated thousands of CTC trajectories initialized near the inlet (Fig. 7) within a digital reconstruction of their bioprinted vessel. The resulting adhesion hotspots are shown in cyan in Fig. 8. WSS-dependent modulation of adhesion was modeled using Model 1, which demonstrated the strongest agreement with prior experimental measurements of WSS-mediated binding dynamics [20], as supported by the results in Figs. 6–4. Cell attachment localized primarily to the bifurcation regions of the entry forks. Additionally, consistent with Hynes et al., more binding events occurred in the lower fork. To determine whether WSS-mediated receptor modulation underlies this asymmetric cell burden, a baseline simulation was performed in which receptor dynamics were not influenced by WSS. Regional enrichment in active receptor levels and bond duration was quantified across simulations, with statistical significance reported in Fig. 9. Under WSS modulation, the lower entry fork exhibited a substantial 31-fold increase in receptors actively engaged in CTC bonds, accompanied by prolonged bond lifetimes. By contrast, the baseline scenario produced only a modest 1.82-fold enrichment. Moreover, in the absence of WSS modulation, mean bond lifetimes were actually higher in the upper fork, indicating a reversal of the WSS-driven pattern.

ICCS Camera Ready Version 2026
To cite this paper please use the final published version:
DOI: 10.1007/978-3-032-29921-5_30

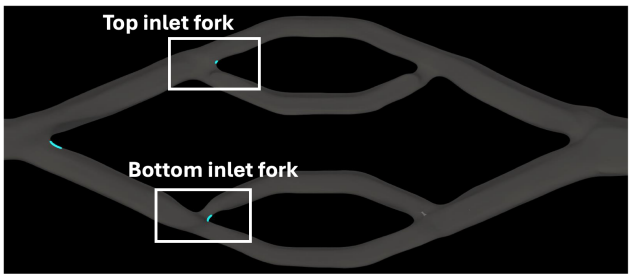

Fig. 8. Spatial locations where cell-wall binding events were recorded in the double bifurcation geometry from [17]. Global binding events observed using Model 1 are colored in cyan.

4 Discussion

We examined whether WSS-regulated adhesion contributes to spatial biases in CTC attachment. WSS magnitude regulation emerged as the dominant driver of adhesive behavior across all geometries tested. Within the curved microvessel domain, Model-1 (Equations 7–8) substantially increased both bond formation frequency (Fig. 6) and engagement duration (Fig. 4), while Model-2 produced no change relative to the baseline. This is consistent with experimental evidence that WSS magnitude strongly enhances adhesive receptor expression, whereas gradient effects remain comparatively modest [20]. Model-3 also elevated bond counts and durations, in line with shear-dependent endothelial signaling responses [38]. While Model-3 is more phenomenological in nature, paracrine communication from upstream WSS stimuli provides a plausible biological basis [3], though the spatial extent and quantitative dependence of this signaling along the vessel axis remain largely unexplored.

The regional preference for metastatic seeding reported experimentally by Hynes et al. [17] was reproduced in our simulations (Fig. 8), enabling direct interrogation of the underlying mechanism. Comparison between baseline (non-WSS modulated) and WSS-regulated adhesion (Fig. 9C) revealed that spatial variations in WSS within bifurcation entry forks are sufficient to generate the observed asymmetry in attachment. With WSS modulation, the lower entry fork exhibited a significantly greater enrichment of receptors actively engaged in CTC bonding than in the baseline condition, consistent with the experimentally observed increase in attachment frequency. Together, these findings provide mechanistic evidence that local WSS cues directly drive spatial bias in CTC binding within complex vascular geometries. Of the three schemes, Model 1 best reproduced the experimental data, capturing the regional asymmetry in attachment and the receptor engagement trends reported by Hynes et al. Model 2 produced adhesive behavior indistinguishable from the unregulated baseline whereas, Model 3 increased bond counts and durations, though its mechanistic basis is less well-characterized.

ICCS Camera Ready Version 2026
To cite this paper please use the final published version:
DOI: 10.1007/978-3-032-29921-5_30

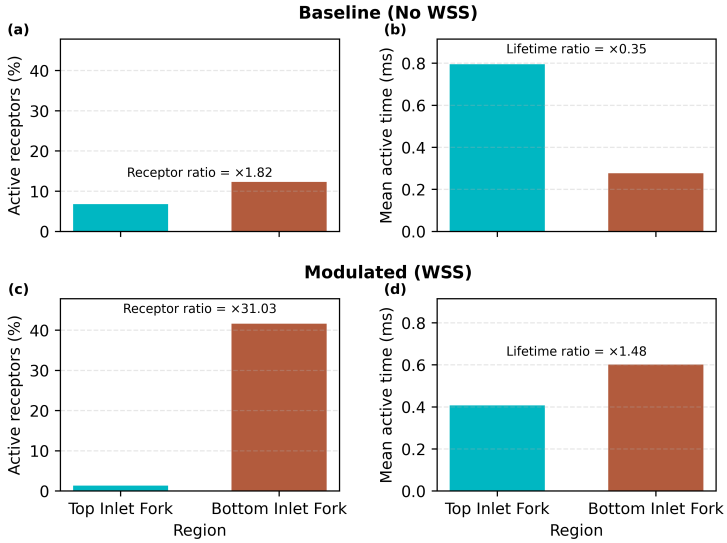

Fig. 9. Quantifying differential cell attachment dynamics between upper and lower entry forks of the bioprinted vasculature from Hynes et al. [17] under the hypothesis of (A): WSS does not impact adhesive dynamics, and (B): WSS modulation of adhesive dynamics is permitted. In both cases, the left-hand column evaluates the fold change in active receptors between the upper and lower inlet forks, and the right-hand column evaluates the fold-change in average bond lifetime.

Several aspects of the modeling scope warrant further exploration. The present simulations do not include CTC induced perturbations to the local shear field, despite evidence that adherent cells can locally elevate endothelial WSS over several cell diameters [8]. Incorporating such feedback may further amplify localized adhesion effects. In addition, the adhesion kinetics was restricted to a weak slip bond formulation. Extending the framework to include two pathway catch slip dynamics could enable more detailed investigation of cell type specific adhesive responses under varying shear conditions. Although experimental studies have reported the presence of circulating tumor cell groups [17], this work focused on individual cells with uniform mechanical properties. Accounting for mechanical heterogeneity within a CTC population may further modulate binding behavior [21]. Finally, endothelial receptor expression was assumed spatially uniform, whereas localized expression patterns are known to influence metastatic transport [29].

5 Conclusion

Using a high throughput multiscale computational platform, we directly evaluated whether WSS regulated adhesion contributes to spatial biases in metastatic

ICCS Camera Ready Version 2026
To cite this paper please use the final published version:
DOI: 10.1007/978-3-032-29921-5_30

seeding. Across tissue scale vascular networks, incorporating WSS dependent adhesive kinetics led to marked increases in receptor engagement and bond lifetime within high WSS inlet regions relative to a non WSS baseline. The dominant sensitivity of adhesion dynamics to the magnitude of the WSS is consistent with established experimental observations [20] and enables a mechanistic explanation for regional attachment preferences reported in bioprinted vascular models. Beyond reproducing observed trends, this framework provides a scalable approach to investigating how local hemodynamics influence metastatic transport at a population scale, opening the door to predictive studies of CTC arrest in realistic vascular networks.

6 Acknowledgements

The authors thank Wentao Ma and Jorik Stoop for fruitful discussions. The authors would also like to thank William Ladd for assisting in the visualizations in Fig. 7. This work was supported by the NCI of the NIH under Award Number 5R01EB024989. Research reported in this publication was supported by the NIH under Award Number T32GM144291. Computing support for this work came from the Argonne National Laboratory (ANL) Aurora Early Science program. An award of computer time was provided by the INCITE program. This research used resources of the Argonne Leadership Computing Facility, which is a DOE Office of Science User Facility supported under Contract DE-AC02-06CH11357.

References

1. Anderson, R.L., Balasas, T., Callaghan, J., Coombes, R.C., Evans, J., Hall, J.A., Kinrade, S., Jones, D., Jones, P.S., Jones, R., et al.: A framework for the development of effective anti-metastatic agents. Nature Reviews Clinical Oncology **16**(3), 185–204 (2019)
2. Anderson, W.K., Bonhaus, D.L.: An implicit upwind algorithm for computing turbulent flows on unstructured grids. Computers & Fluids **23**(1), 1–21 (1994)
3. Bertani, F., Di Francesco, D., Corrado, M.D., Talmon, M., Fresu, L.G., Boccafoschi, F.: Paracrine shear-stress-dependent signaling from endothelial cells affects downstream endothelial function and inflammation. International Journal of Molecular Sciences **22**(24), 13300 (2021)
4. Bhatnagar, P.L., Gross, E.P., Krook, M.: A model for collision processes in gases. I. Small amplitude processes in charged and neutral one-component systems. Phys. Rev. **94**(3), 511–525 (1954)
5. Casas-Arozamena, C., Otero-Cacho, A., Carnero, B., Almenglo, C., Aymerich, M., Alonso-Alconada, L., Ferreiros, A., Abalo, A., Bao-Varela, C., Flores-Arias, M.T., et al.: Haemodynamic-dependent arrest of circulating tumour cells at large blood vessel bifurcations as new model for metastasis. Scientific Reports **11**(1), 23231 (2021)
6. Costa-Silva, B., Aiello, N.M., Ocean, A.J., Singh, S., Zhang, H., Thakur, B.K., Becker, A., Hoshino, A., Mark, M.T., Molina, H., et al.: Pancreatic cancer exosomes initiate pre-metastatic niche formation in the liver. Nature cell biology **17**(6), 816–826 (2015)

ICCS Camera Ready Version 2026
To cite this paper please use the final published version:
DOI: 10.1007/978-3-032-29921-5_30

7. Coughlin, M.F., Kamm, R.D.: The use of microfluidic platforms to probe the mechanism of cancer cell extravasation. Advanced Healthcare Materials **9**(8), 1901410 (2020)
8. Dabagh, M., Randles, A.: Role of deformable cancer cells on wall shear stress-associated-vegf secretion by endothelium in microvasculature. PloS one **14**(2), e0211418 (2019)
9. Dolan, J.M., Meng, H., Sim, F.J., Kolega, J.: Differential gene expression by endothelial cells under positive and negative streamwise gradients of high wall shear stress. American Journal of Physiology-Cell Physiology **305**(8), C854–C866 (2013)
10. Ewing, J.: Neoplastic diseases: a treatise on tumors. Wb saunders (1928)
11. Fedosov, D., Caswell, B., Suresh, S., Karniadakis, G.: Quantifying the biophysical characteristics of plasmodium-falciparum-parasitized red blood cells in microcirculation. Proceedings of the National Academy of Sciences **108**(1), 35–39 (2011)
12. Fitzgerald, D.P., Palmieri, D., Hua, E., Hargrave, E., Herring, J.M., Qian, Y., Vega-Valle, E., Weil, R.J., Stark, A.M., Vortmeyer, A.O., et al.: Reactive glia are recruited by highly proliferative brain metastases of breast cancer and promote tumor cell colonization. Clinical & experimental metastasis **25**(7), 799–810 (2008)
13. Fournier, P.G., Juárez, P., Jiang, G., Clines, G.A., Niewolna, M., Kim, H.S., Walton, H.W., Peng, X.H., Liu, Y., Mohammad, K.S., et al.: The tgf-β signaling regulator pmepa1 suppresses prostate cancer metastases to bone. Cancer cell **27**(6), 809–821 (2015)
14. Gijsen, F., Katagiri, Y., Barlis, P., Bourantas, C., Collet, C., Coskun, U., Daemen, J., Dijkstra, J., Edelman, E., Evans, P., et al.: Expert recommendations on the assessment of wall shear stress in human coronary arteries: existing methodologies, technical considerations, and clinical applications. European heart journal **40**(41), 3421–3433 (2019)
15. Gupta, G.P., Perk, J., Acharyya, S., De Candia, P., Mittal, V., Todorova-Manova, K., Gerald, W.L., Brogi, E., Benezra, R., Massagué, J.: Id genes mediate tumor reinitiation during breast cancer lung metastasis. Proceedings of the National Academy of Sciences **104**(49), 19506–19511 (2007)
16. Hammer, D.A., Apte, S.M.: Simulation of cell rolling and adhesion on surfaces in shear flow: general results and analysis of selectin-mediated neutrophil adhesion. Biophysical journal **63**(1), 35–57 (1992)
17. Hynes, W., Pepona, M., Robertson, C., Alvarado, J., Dubbin, K., Triplett, M., Adorno, J., Randles, A., Moya, M.L.: Examining metastatic behavior within 3d bioprinted vasculature for the validation of a 3d computational flow model. Science advances **6**(35), eabb3308 (2020)
18. Kim, S., Wan, Z., Jeon, J.S., Kamm, R.D.: Microfluidic vascular models of tumor cell extravasation. Frontiers in Oncology **12**, 1052192 (2022)
19. Krüger, T., Varnik, F., Raabe, D.: Efficient and accurate simulations of deformable particles immersed in a fluid using a combined immersed boundary lattice boltzmann finite element method. Computers & Mathematics with Applications **61**(12), 3485–3505 (2011)
20. LaMack, J.A., Friedman, M.H.: Individual and combined effects of shear stress magnitude and spatial gradient on endothelial cell gene expression. American Journal of Physiology-Heart and Circulatory Physiology **293**(5), H2853–H2859 (2007)
21. Lv, J., Liu, Y., Cheng, F., Li, J., Zhou, Y., Zhang, T., Zhou, N., Li, C., Wang, Z., Ma, L., et al.: Cell softness regulates tumorigenicity and stemness of cancer cells. The EMBO journal **40**(2), e106123 (2021)

ICCS Camera Ready Version 2026
To cite this paper please use the final published version:
DOI: 10.1007/978-3-032-29921-5_30

22. Marshall, B.T., Long, M., Piper, J.W., Yago, T., McEver, R.P., Zhu, C.: Direct observation of catch bonds involving cell-adhesion molecules. Nature **423**(6936), 190–193 (2003)
23. Martin, A., Ladd, W., Wu, R., Randles, A.: Adaptive physics refinement enables high-throughput, tissue-scale adhesive dynamics simulations. In: Journal of Computational Science (under review). Springer (2025)
24. Martin, A., Ladd, W., Wu, R., Randles, A.: Adaptive physics refinement for anatomic adhesive dynamics simulations. In: International Conference on Computational Science. pp. 268–282. Springer (2025)
25. Nan, J., Roychowdhury, S., Randles, A.: Investigating the influence of heterogeneity within cell types on microvessel network transport. Cellular and Molecular Bioengineering **16**(5), 497–507 (2023)
26. Paget, S.: The distribution of secondary growths in cancer of the breast. The Lancet **133**(3421), 571–573 (1889)
27. Peskin, C.S.: Numerical analysis of blood flow in the heart. Journal of Computational Physics **25**(3), 220–252 (1977)
28. Popel, A.S., Johnson, P.C.: Microcirculation and hemorheology. Annu. Rev. Fluid Mech. **37**(1), 43–69 (2005)
29. Puleri, D.F., Randles, A.: The role of adhesive receptor patterns on cell transport in complex microvessels. Biomechanics and modeling in mechanobiology **21**(4), 1079–1098 (2022)
30. Puleri, D.F., Roychowdhury, S., Balogh, P., Gounley, J., Draeger, E.W., Ames, J., Adebiyi, A., Chidyagwai, S., Hernández, B., Lee, S., et al.: High performance adaptive physics refinement to enable large-scale tracking of cancer cell trajectory. In: 2022 IEEE International Conference on Cluster Computing (CLUSTER). pp. 230–242. IEEE (2022)
31. Qian, Y.H., d'Humières, D., Lallemand, P.: Lattice bgk models for navier-stokes equation. Europhysics letters **17**(6), 479 (1992)
32. Randles, A.P., Kale, V., Hammond, J., Gropp, W., Kaxiras, E.: Performance analysis of the lattice boltzmann model beyond navier-stokes. In: 2013 IEEE 27th International Symposium on Parallel and Distributed Processing. pp. 1063–1074. IEEE (2013)
33. Sarangapani, K.K., Marshall, B.T., McEver, R.P., Zhu, C.: Molecular stiffness of selectins. Journal of Biological Chemistry **286**(11), 9567–9576 (2011)
34. Skalak, R., Tozeren, A., Zarda, R., Chien, S.: Strain energy function of red blood cell membranes. Biophysical journal **13**(3), 245–264 (1973)
35. Takeishi, N., Imai, Y., Ishida, S., Omori, T., Kamm, R.D., Ishikawa, T.: Cell adhesion during bullet motion in capillaries. American Journal of Physiology-Heart and Circulatory Physiology **311**(2), H395–H403 (2016)
36. Xiao, L., Liu, Y., Chen, S., Fu, B.: Effects of flowing rbcs on adhesion of a circulating tumor cell in microvessels. Biomechanics and modeling in mechanobiology **16**(2), 597–610 (2017)
37. Xie, X., Wang, F., Zhu, L., Yang, H., Pan, D., Liu, Y., Qu, X., Gu, Y., Li, X., Chen, S.: Low shear stress induces endothelial cell apoptosis and monocyte adhesion by upregulating pecam-1 expression. Molecular Medicine Reports **21**(6), 2580–2588 (2020)
38. Yan, W., Cai, B., Liu, Y., Fu, B.: Effects of wall shear stress and its gradient on tumor cell adhesion in curved microvessels. Biomechanics and modeling in mechanobiology **11**, 641–653 (2012)

ICCS Camera Ready Version 2026
To cite this paper please use the final published version:
DOI: 10.1007/978-3-032-29921-5_30